Balancing and Velocity Control of a Unicycle Robot Based on the Dynamic Model

Seong I. Han, *Member, IEEE*, and Jang M. Lee, *Senior Member, IEEE*

***Abstract*—This paper presents a dynamic-model-based control scheme for the balancing and velocity control of a unicycle robot. Unicycle robot motion consists of a pitch that is controlled by an in-wheel motor and a roll that is controlled by a reaction wheel pendulum. The unicycle robot lacks an actuator for yaw-axis control, which makes the derivation of the dynamics relatively simple although it may limit the motion control. The Euler–Lagrange equation is applied to derive the dynamic equations of the unicycle robot to implement dynamic speed control. To achieve real-time speed control, a sliding-mode control and a nonzero set-point linear quadratic regulator (LQR) are utilized to guarantee stability while maintaining the desired speed-tracking performance. In the roll controller, a sigmoid-function-based sliding-mode controller has been adopted to minimize switching-function chattering. An LQR controller has been implemented for pitch control to drive the unicycle robot to follow the desired velocity trajectory in real time using the state variables of pitch angle, angular velocity, wheel angle, and angular velocity. The control performance of the two control systems using a single dynamic model has been experimentally demonstrated.**

***Index Terms*—Dynamic equation, nonzero set-point linear quadratic regulator (LQR), sliding-mode control, unicycle robot, velocity and trajectory control.**

I. Introduction

RESEARCH on the single-wheel (unicycle) robot has been under way since the 1980s in the USA and Japan [1], [2]. A. Schoonwinkel of Stanford University proposed a linear dynamic model for the robot and presented its optimal motion control [3], [4]. A professor of Tokyo University also proposed a dynamic model for the robot that comprised an upper turntable and a lower rotating wheel [5]. Honda developed UX-3 as a personal mobility system, and Murata Manufacturing Company Ltd., also developed Murata Girl on a single wheel. Most of the research on the single-wheel robot has focused on the stable driving of the single wheel without considering specific types of trajectory control. Currently, there is a study that implements trajectory control assuming that the dynamics of the upper reaction wheel pendulum and the lower inverted pendulum are decoupled [6]. In the study, the coupling terms are compensated by an intelligent algorithm such as fuzzy interference. For the high-speed motion of the single-wheel robot, the coupling terms become large and time varying. Therefore, the intelligent algorithm is not adequate for various trajectory controls [7]–[9]. As the applications of a unicycle robot, Murata Manufacturing Company Ltd., exhibited a robot riding a unicycle named "Murata Girl" in September 2008 [10]. Human riding a unicycle model [11] and similar types of unicycle robots have been developed [12]–[14]. Air blowing and magnetic-force-balanced unicycle models are studied instead of disk rotation for the side balancing of a unicycle robot [15], [16].

In this paper, a new unicycle robot is designed and implemented. After deriving the dynamic equations of the unicycle robot, which is expressed as a 3-D model structure, a model-based controller is designed to maintain balance and to drive the unicycle robot to a desired location. Since the dynamic characteristics of the roll and pitch axes are different, two different controllers are designed for the balance of the roll axis and for the speed control of the pitch axis. First, the sliding-mode control is applied to the roll axis [17]–[21]. When a controlled variable of the sliding-mode control meets the Lyapunov stability condition, the controller can stably maintain the control states. In designing the sliding-mode controller, the key issue is to find appropriate controlled variables. The chattering problem of the sliding-mode control, which used the signum function as a switching function, is also resolved in this paper. The chattering phenomenon damages actuators and disturbs the system states. Thus, the chattering must be attenuated to an acceptable level. In this paper, first, the chattering is greatly reduced by using a sigmoidal function such as the tanh function. Second, the nonzero set-point linear quadratic regulator (LQR) [22], [23] is designed with the weighting matrices for pitch-axis control. With this LQR controller, the balance and speed controls are operated concurrently.

After this introduction, system modeling is expressed in Section II. In Section III, the design of the control system is illustrated in detail. The results of experiments are demonstrated in Section IV, and finally, in Section V, the conclusions and future research works are summarized and suggested.

II. System Modeling

In this section, the dynamic equations of the unicycle robot are derived. In Fig. 1, the disk is installed on the top to generate rotational inertia, and the central axis of the disk is maintained as the center of gravity. Therefore, the upper part of

Manuscript received December 8, 2013; revised March 20, 2014; accepted May 10, 2014. Date of publication June 2, 2014; date of current version December 19, 2014. This work was supported by the National Research Foundation of Korea Grant funded by the Korean Government (Ministry of Science, ICT and Future Planning) under Grant NRF-2013R1A1A 2021174.

The authors are with the Department of Electronics Engineering, College of Engineering, Pusan National University, Busan 609-735, Korea (e-mail: skhan@pusan.ac.kr; jmlee@pusan.ac.kr).

Color versions of one or more of the figures in this paper are available online at http://ieeexplore.ieee.org.

Digital Object Identifier 10.1109/TIE.2014.2327562

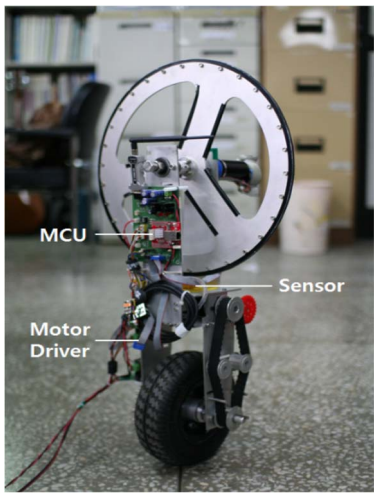

Fig. 1. Unicycle robot.

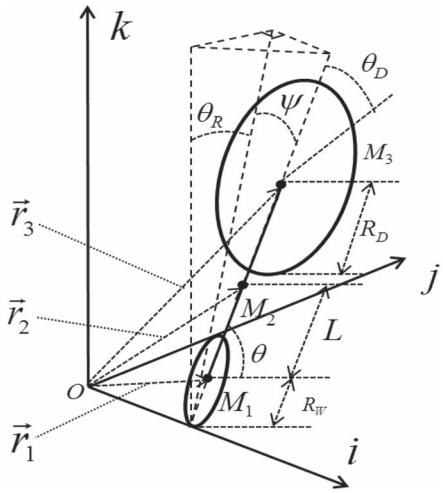

Fig. 2. Structure map of the unicycle robot.

the unicycle is a reaction wheel pendulum, and the lower part can be modeled as an inverted pendulum.

There are a few methods that can be used to obtain the dynamic equations of a system. In this paper, the Lagrange equation is used to derive the dynamic equations, which can be used for the design of the simulation and control systems.

A structure map of the unicycle robot is defined and drawn in 3-D space to reveal the physical characteristics of the unicycle robot for the dynamic model. The reference axis is set as $\{i, j, k\}$ in Fig. 2, where L represents the length from the center of the wheel to the center of the body. R_D and R_w denote the radii of the disk and the wheel, respectively. θ_R represents the angle of the roll axis, and θ defines the angle of the wheel. ψ and θ_D denote the angles of the pitch axis and the disk, respectively. M_1, M_2, and M_3 denote the masses of the wheel, body, and disk, respectively [24].

Generally, to obtain the dynamic equations from the Lagrange equation, the kinetic and potential energy terms are required. Kinetic energy consists of translational kinetic energy and rotational kinetic energy. First, position vectors are defined to obtain the translational kinetic energy. In Fig. 2, $\vec{r}_1$, $\vec{r}_2$, and $\vec{r}_3$ represent the position vectors of the wheel, body, and disk, respectively, and are defined as follows:

$$\vec{r}_1 = R_w\theta\hat{i} + R_w s\theta_R\hat{j} + R_w c\theta_R\hat{k} \tag{1}$$

$$\vec{r}_2 = (R_w\theta + Ls\psi)\hat{i} + (R_w s\theta_R + Lc\psi s\theta_R)\hat{j} + (R_w c\theta_R + Lc\psi c\theta_R)\hat{k} \tag{2}$$

$$\vec{r}_3 = (R_w\theta + 2Ls\psi)\hat{i} + (R_w s\theta_R + 2Lc\psi s\theta_R)\hat{j} + (R_w c\theta_R + 2Lc\psi c\theta_R)\hat{k} \tag{3}$$

where $s(\cdot)$ and $c(\cdot)$ mean $\sin(\cdot)$ and $\cos(\cdot)$, respectively. From the position vectors, the velocity vectors are obtained as follows:

$$\vec{v}_1 = R_w\dot{\theta}\hat{i} + R_w\dot{\theta}_R c\theta_R\hat{j} - R_w\dot{\theta}_R s\theta_R\hat{k} \tag{4}$$

$$\vec{v}_2 = (L\dot{\psi}c\psi + R_w\dot{\theta})\hat{i} + (-L\dot{\psi}s\psi s\theta_R + R_w\dot{\theta}_R c\theta_R + L\dot{\theta}_R c\psi c\theta_R)\hat{j} + (-L\dot{\psi}c\theta_R s\psi - R_w\dot{\theta}_R s\theta_R - L\dot{\theta}_R s\psi s\theta_R)\hat{k} \tag{5}$$

$$\vec{v}_3 = (2L\dot{\psi}c\psi + R_w\dot{\theta})\hat{i} + (-2L\dot{\psi}s\psi s\theta_R + R_w\dot{\theta}_R c\theta_R + 2L\dot{\theta}_R c\psi c\theta_R)\hat{j} + (-2L\dot{\psi}c\theta_R s\psi - R_w\dot{\theta}_R s\theta_R - 2L\dot{\theta}_R c\psi s\theta_R)\hat{k}. \tag{6}$$

Total kinetic energy T is obtained as the sum of translational kinetic energy T_1 and rotational kinetic energy T_2 as follows:

$$T = T_1 + T_2 \tag{7}$$

$$T_1 = \frac{1}{2}M_1(\vec{v}_1\cdot\vec{v}_1) + \frac{1}{2}M_2(\vec{v}_2\cdot\vec{v}_2) + \frac{1}{2}M_3(\vec{v}_3\cdot\vec{v}_3) \tag{8}$$

$$T_2 = \frac{1}{2}J_w\dot{\theta}^2 + \frac{1}{2}J_m n^2(\dot{\theta}-\dot{\psi})^2 + \frac{1}{2}J_\psi\dot{\psi}^2 + \frac{1}{2}J_d(\dot{\theta}_R+\dot{\theta}_D)^2. \tag{9}$$

In Fig. 2, the potential energy of the unicycle robot is obtained as

$$U = M_1 g R_w c\theta_R + M_2 g(R_w c\theta_R + Lc\psi c\theta_R) + M_3 g(R_w c\theta_R + 2Lc\psi c\theta_R). \tag{10}$$

The Lagrangian, which is the difference between the kinetic energy and the potential energy, is given by

$$L = T - U. \tag{11}$$

Substituting L into the Lagrange dynamic equation, the dynamic equations of the unicycle robot are obtained as follows:

$$\frac{d}{dt}\left(\frac{\partial L}{\partial\dot{q}}\right) - \frac{\partial L}{\partial q} = \tau_q \tag{12}$$

where $q = [\theta_R\ \theta_D\ \psi\ \theta]^T$. From (9), the dynamic equations of the system states of the unicycle robot are obtained as follows:

$$M(q)\ddot{q} + C(q,\dot{q})\dot{q} + G(q) = \tau_q \tag{13}$$

where

$$M(q) = \begin{bmatrix} M_{11} & M_{12} & M_{13} & 0 \\ M_{21} & M_{22} & 0 & 0 \\ M_{31} & 0 & M_{33} & M_{34} \\ 0 & 0 & M_{43} & M_{44} \end{bmatrix}$$

$$C(q,\dot{q}) = \begin{bmatrix} C_{11} & 0 & C_{13} & 0 \\ 0 & 0 & 0 & 0 \\ C_{31} & 0 & C_{33} & 0 \\ 0 & 0 & C_{43} & 0 \end{bmatrix}$$

$$G(q) = [G_1 \quad 0 \quad G_3 \quad 0]^T$$

$$\tau = [\tau_R \quad \tau_D \quad \tau_\psi \quad \tau_\theta]^T$$

$$\begin{aligned} M_{11} &= M_1 R_w^2 + M_2\left(R_w^2 + L^2c^2\psi c^2\theta_R + 2LR_w c^2\theta_R c\psi \right. \\ &\quad \left. + L^2 s^2\psi s^2\theta_R + 2LR_w s^2\theta_R s\psi\right) \\ &\quad + M_3\left(R_w^2 + 4L^2c^2\psi + 4LR_w c\psi\right) + J_d \\ M_{12} &= M_{21} = J_d \\ M_{13} &= M_{31} = M_2L^2 s\theta_R c\theta_R(-s\psi c\psi + s^2\psi) \\ M_{22} &= J_d \\ M_{33} &= M_2L^2c^2\psi + M_3 4L^2c^2\psi - J_m n^2 + J_\psi \\ M_{34} &= M_{43} = M_2LR_w c\psi + 2M_3LR_w c\psi + J_m n^2 \\ M_{44} &= M_2R_w^2 + M_3R_w^2 + J_w + J_m n^2 \\ C_{11} &= M_2(-L^2c^2\psi c\theta_R s\theta_R - 2LR_w c\theta_R s\theta_R c\psi \\ &\quad + L^2 s^2\psi s\theta_R c\theta_R)\dot{\theta}_R \\ &\quad + \left[M_2(-L^2 c\psi s\psi c^2\theta_R \right. \\ &\quad \left. + L^2 s^2\psi s\theta_R c\theta_R + LR_w s^2\theta_R c\psi) \right. \\ &\quad \left. + M_3\left(-4L^2 c\psi s\psi - 2LR_w s\psi\right)\right]\dot{\psi} \\ C_{13} &= \left[M_2\left(-L^2 c\psi s\psi c^2\theta_R - LR_w c^2\theta_R s\psi \right.\right. \\ &\quad \left. + L^2 s\psi c\psi s^2\theta_R + LR_w s^2\theta_R c\psi\right) \\ &\quad \left. + M_3\left(-4L^2 c\psi s\psi - 2LR_w s\psi\right)\right]\dot{\theta}_R \\ &\quad + M_2L^2(c^2\theta_R - s^2\theta_R)(-s\psi c\psi + s^2\psi)\dot{\psi} \\ C_{31} &= \left[M_2L^2(c^2\theta_R - s^2\theta_R)\left(-s\psi c\psi + s^2\psi\right)\right. \\ &\quad - M_2\left(-L^2 c\psi s\psi c^2\theta_R - LR_w c^2\theta_R s\psi \right. \\ &\quad \left.\left. + L^2 s\psi c\psi s^2\theta_R + LR_w s^2\theta_R c\psi\right)\right]\dot{\theta}_R \\ C_{33} &= (-M_2L^2 c\psi s\psi - 4M_3L^2 c\psi s\psi)\dot{\psi} \\ C_{43} &= (-M_2LR_w s\psi - 2M_3LR_w s\psi)\dot{\psi} \end{aligned}$$

τ_R, τ_D, τ_ψ, and τ_θ represent the torques on the roll axis, disk, pitch axis, and wheel, respectively. According to the law of conservation of angular momentum, there are two constraint equations in each set of two torques, i.e., $\tau_R = -\tau_D$ and $\tau_\psi = -\tau_\theta$.

Since the motor drives are controlled by pulsewidth modulation (PWM), the torque inputs are required to be transformed to voltage inputs. The dynamic equations that express the torque inputs can be transformed to express the voltage inputs by using the dynamic equations of dc motors. The torque of a roll dc motor can be represented by the voltage as follows:

$$\tau_\theta = \frac{nk_t}{R_m}V - \left(\frac{nk_t}{R_m}k_b + f_m\right)(\dot{\theta} - \dot{\psi}) \tag{14}$$

$$\tau_D = \frac{nk_t}{R_m}V - \left(\frac{nk_t}{R_m}k_b + f_m\right)(\dot{\theta}_D - \dot{\theta}_R) \tag{15}$$

TABLE I
UNICYCLE ROBOT PARAMETERS

Symbol	Parameter	Quantity
M_1, M_2, M_3	mass of wheel, body and disc	1.43kg, 4.08kg, 1.30kg
R_w, R_D	radius of wheel and disc	0.11m, 0.20m
L	length from the center of the wheel to the center of body	0.225m
g	gravity acceleration	9,806m/s^2
J_d	inertia of the disc	0.1840kgm^2
J_ψ	inertia of the robot body and the rotational disc	0.1951kgm^2
J_w	inertia of the wheel	0.0086kgm^2
J_m	inertia of the motor armature	0.0001kgm^2
J_b	inertia of the robot body and the wheel	0.0928kgm^2

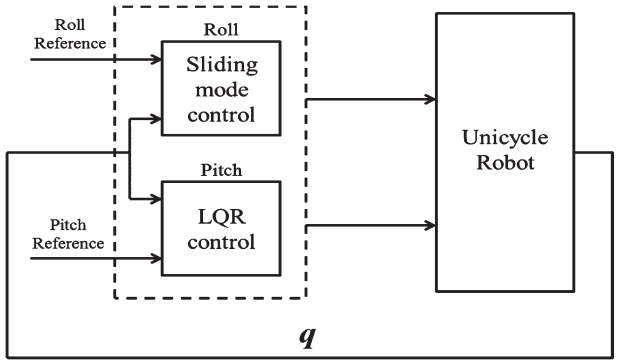

Fig. 3. Block diagram of the overall system.

where V is the input voltage of the roll axis motor, n is the motor gear ratio, R_m is the resistor coefficient of the motor, k_t denotes the torque constant, f_m denotes the friction coefficient of the motor, and k_b denotes the back-electromotive-force constant. Notice that the same motors and gears are used for the roll and pitch controllers. Therefore, the torque of the pitch and that of the roll motor can be directly obtained as $\tau_\psi = -\tau_\theta$ and $\tau_R = -\tau_D$, respectively. For simplicity, (nk_t/R_m) and $(nk_t/R_m)k_b + f_m$ are renamed as α and β, respectively. In the design process of the controller for each axis, α and β are differently determined for each controller. Table I indicates the parameter values used in the dynamic equations.

III. CONTROLLER DESIGN

In this section, the controllers are designed based on the dynamic equations of the robot obtained in the previous section. The unicycle robot has two actuators that are separately located on the roll and pitch axes, and the controller design for these actuators is the major goal in this section. From previous experience with controlling this unicycle robot, the sliding-mode controller and the nonzero set-point LQR controller are selected for the roll and pitch axes, respectively. Fig. 3 depicts the overall system block diagram of the unicycle robot. The states of the unicycle robot are defined as $\boldsymbol{q} = [\theta_R\ \dot{\theta}_R\ \theta_D\ \dot{\theta}_D\ \psi\ \dot{\psi}\ \theta\ \dot{\theta}]^T$. The system controllers of the sliding-mode control for the roll and the LQR control for the pitch are placed in front of the system. The outputs of the controllers enter the system to control the

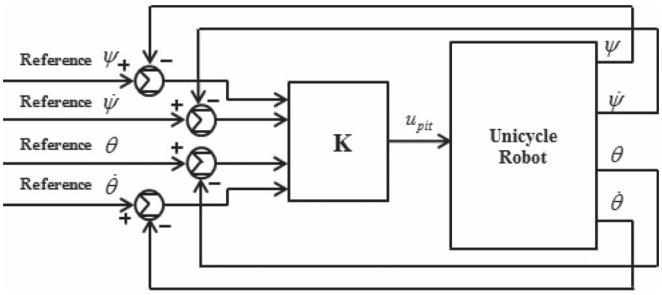

Fig. 4. Block diagram of the LQR control for the pitch controller.

actuators. Different references are specified for each axis of the roll and the pitch. The balance control is only implemented at the roll axis, whereas both the balance and driving controls are conducted at the pitch axis.

A. Pitch Controller

Fig. 4 shows the control block diagram of the designed nonzero set-point LQR controller for controlling the pitch axis. K is defined as $[K_1, K_2, K_3, K_4]$ for each of the four inputs. There are two references to control balance and driving simultaneously. Reference ψ is used for balance control, and reference θ is used for driving control.

To apply this state-feedback optimal control, first, a system matrix and weight matrices need to be determined as follows:

$$\dot{x}_p = A_p x_p + B_p u_p \tag{16}$$

where the system states are defined as $x_p = [\psi\ \dot{\psi}\ \theta\ \dot{\theta}]^T$, u_p represents the input voltages, which are obtained from the dynamic equations expressed in terms of the voltage inputs. These equations can be derived by transforming the torques to voltages by using dc-motor dynamic equations.

The simplified pitch dynamics can be represented as follows:

$$\begin{aligned}\ddot{\psi} = &\Big[\left(M_2R_w^2+M_3R_w^2+J_w+J_mn^2\right)\left(-M_2L^2\psi-4M_3L^2\psi\right)\dot{\psi}^2\\ &-\left(M_2LR_w+2M_3LR_w+J_mn^2\right)\\ &\times\left(-M_2R_wL\psi-2M_3LR_w\psi\right)\dot{\psi}^2\\ &+\left(M_2R_w^2+M_3R_w^2+J_w+J_mn^2\right)\left(M_2gL+2M_3gL\right)\psi\\ &+\left(-M_2R_w^2-M_3R_w^2-J_w-M_2LR_w\right.\\ &\left.-2M_3LR_w-2J_mn^2\right)\left(\alpha V-\beta(\dot{\theta}-\dot{\psi})\right)\Big]\\ &/\left[\left(M_2R_w^2+M_3R_w^2+J_w+J_mn^2\right)\right.\\ &\times\left(M_2L^2+M_34L^2-J_mn^2+J_\psi\right)\\ &\left.-\left(M_2LR_w+2M_3LR_w+J_mn^2\right)^2\right]\end{aligned} \tag{17}$$

$$\begin{aligned}\ddot{\theta} = &\Big[-\left(M_2LR_w+2M_3LR_w+J_mn^2\right)\\ &\times\left(-M_2L^2\psi-4M_3L^2\psi\right)\dot{\psi}^2\\ &+\left(M_2L^2+M_34L^2-J_mn^2+J_\psi\right)\\ &\times\left(-M_2LR_w\psi-2M_3LR_w\psi\right)\dot{\psi}^2\\ &-\left(M_2LR_w+2M_3LR_w+J_mn^2\right)\left(M_2gL+2M_3gL\right)\psi\\ &+\left(M_2LR_w+2M_3LR_w+M_2L^2+4M_3L^2+J\psi\right)\\ &\times\left(\alpha V+\beta(\dot{\theta}-\dot{\psi})\right)\Big]\\ &/\left[\left(M_2R_w^2+M_3R_w^2+J_w+J_mn^2\right)\right.\\ &\times\left(M_2L^2+M_34L^2-J_mn^2+J_\psi\right)\\ &\left.-\left(M_2LR_w+2M_3LR_w+J_mn^2\right)^2\right].\end{aligned} \tag{18}$$

Equations (17) and (18) can be arranged to obtain the A and B matrices in the following equation, which represents the resulting system matrix:

$$\begin{bmatrix}\dot{\psi}\\ \ddot{\psi}\\ \dot{\theta}\\ \ddot{\theta}\end{bmatrix} = \begin{bmatrix}0 & 1 & 0 & 0\\ A_{21} & A_{22} & 0 & A_{24}\\ 0 & 0 & 0 & 1\\ A_{41} & A_{42} & 0 & A_{44}\end{bmatrix}\begin{bmatrix}\psi\\ \dot{\psi}\\ \theta\\ \dot{\theta}\end{bmatrix} + \begin{bmatrix}0\\ B_{21}\\ 0\\ B_{41}\end{bmatrix} u_{\text{pit}} \tag{19}$$

where

$$\begin{aligned}A_{21} &= \left(M_2R_w^2+M_3R_w^2+J_w+J_mn^2\right)\left(M_2+2M_3\right)gL/D_{\text{pit}}\\ A_{22} &= \left(M_2R_w^2+M_3R_w^2+J_w+J_mn^2\right)\\ &\quad\times\left(-M_2L^2\psi-4M_3L^2\psi\right)\dot{\psi}\\ &\quad-\left(M_2R_wL+2M_3LR_w+J_mn^2\right)\\ &\quad\times\left(-M_2R_wL\psi-2M_3LR_w\psi\right)\dot{\psi}\\ &\quad+\left(-M_2R_w^2-M_3R_w^2-J_w-M_2R_wL\right.\\ &\qquad\left.-2M_3LR_w-2J_mn^2\right)\beta/D_{\text{pit}}\\ A_{24} &= -\left(-M_2R_w^2-M_3R_w^2-J_w-M_2LR_w\right.\\ &\qquad\left.-2M_3LR_w-2J_mn^2\right)\beta/D_{\text{pit}}\\ A_{41} &= -\left(M_2LR_w+2M_3LR_w+J_mn^2\right)\\ &\quad\times\left(M_2+2M_3\right)gL/D_{\text{pit}}\\ A_{42} &= -\left(M_2LR_w+2M_3LR_w+J_mn^2\right)\\ &\quad\times\left(-M_2L^2\psi-4M_3L^2\psi\right)\dot{\psi}\\ &\quad+\left(M_2L^2+M_34L^2-J_mn^2+J_\psi\right)\\ &\quad\times\left(-M_2LR_w\psi+M_2L^2-2M_3LR_w\psi\right)\dot{\psi}\\ &\quad-\left(M_2LR_w+2M_3LR_w+4M_3L^2+J_\psi\right)\beta/D_{\text{pit}}\\ A_{44} &= \left(M_2LR_w+2M_3LR_w+M_2L^2+4M_3L^2+J_\psi\right)\beta/D_{\text{pit}}\\ B_{21} &= \left(-M_2R_w^2-M_3R_w^2-J_w-M_2LR_w\right.\\ &\qquad\left.-2M_3LR_w-2J_mn^2\right)\alpha/D_{\text{pit}}\\ B_{41} &= \left(M_2LR_w+2M_3LR_w+M_2L^2+4M_3L^2+J_\psi\right)\alpha/D_{\text{pit}}\\ D_{\text{pit}} &= \left(M_2R_w^2+M_3R_w^2+J_w+J_mn^2\right)\\ &\quad\times\left(M_2L^2+M_34L^2-J_mn^2+J_\psi\right)\\ &\quad-\left(M_2LR_w+2M_3LR_w+J_mn^2\right)^2.\end{aligned}$$

The desired set point is given as

$$x = x_d. \tag{20}$$

Then, $\exists u_d$ is chosen such that

$$\dot{x}_d = Ax_d + Bu_d. \tag{21}$$

We can define the error variables, i.e., $\tilde{u} = u_p - u_d$ and $\tilde{x} = x - x_d$, which satisfy $\dot{\tilde{x}} = A\tilde{x} + B\tilde{u}$.

The LQR control is one of the optimal control methods, and it requires finding an optimal state-feedback gain that minimizes the performance index. The performance index is defined as follows [22], [23]:

$$J = \int_0^\infty \left[\tilde{x}(t)^T Q\tilde{x}(t) + \tilde{u}(t)^T R\tilde{u}(t)\right] dt \tag{22}$$

where Q and R are weight matrices that are key factors in determining the performance of the optimal control.

State-feedback control inputs are expressed as follows:

$$\tilde{u}(t) = -K\tilde{x}(t) \tag{23}$$

where the state-feedback gains are obtained as $K = R^{-1}B^T P$, and P will be uniquely determined as a solution of the Riccati equation as follows:

$$A^T P + PA - PBR^{-1}B^T P + Q = 0. \tag{24}$$

From this Riccati equation, the P matrix is uniquely determined, and it is used to calculate state-feedback gain K. Thus, the control input can be obtained from (24) as follows:

$$u_p = -K\tilde{x} + u_d \tag{25}$$

where u_d contains the command input. Now, for the optimal LQR control, matrices R and Q are required to be defined for application to the Riccati equation. R is selected as an identity matrix, and Q is selected through several trial-and-error experiments as follows:

$$Q = \begin{bmatrix} 150 & 0 & 0 & 0 \\ 0 & 5 & 0 & 0 \\ 0 & 0 & 5 & 0 \\ 0 & 0 & 0 & 25 \end{bmatrix}. \tag{26}$$

For the given A, B, R, and Q matrices, the optimal state-feedback control is determined by solving the Riccati equation as follows:

$$K = [-124.1 \quad -37.8 \quad -2.2 \quad -6.6]. \tag{27}$$

B. Roll controller

The sliding-mode control is known as a robust algorithm, which can properly control nonlinear and uncertain systems characterized by parameter variations, disturbances, and modeling errors. For the roll control, the robust sliding-mode controller is adopted in this paper. The nonlinear roll dynamic model for the unicycle robot is given as

$$\ddot{\theta}_R = f(\theta_R, \dot{\theta}_R) + g_{\text{roll}} u_{\text{roll}} + F_u \tag{28}$$

where $g_{\text{roll}} = -2\alpha J_d / D_{\text{roll}}$, $D_{\text{roll}} = [(M_1 R_w^2 + M_2(R_w^2 + L^2 + 2LR_w) + M_3(R_w^2 + 4L^2 + 4LR_w) + J_d)J_d - J_d^2]$, u_{roll} and $f(\theta_R, \dot{\theta}_R)$ are given in (29) and (33), respectively, and F_u denotes the uncertainties of the system, including the modeling error and the external disturbance given in (33). Notice that F_u can be compensated by u_s, which is called a robust control input.

The control input of the sliding-mode control can be represented as the sum of the equivalent and robust inputs as follows:

$$u_{\text{roll}} = u_{\text{eq}} + u_s \tag{29}$$

where u_{eq} and u_s are defined in (34) and (35), respectively. The foregoing design process is applied to design the sliding-mode control of the roll axis of the unicycle robot. Fig. 5 shows

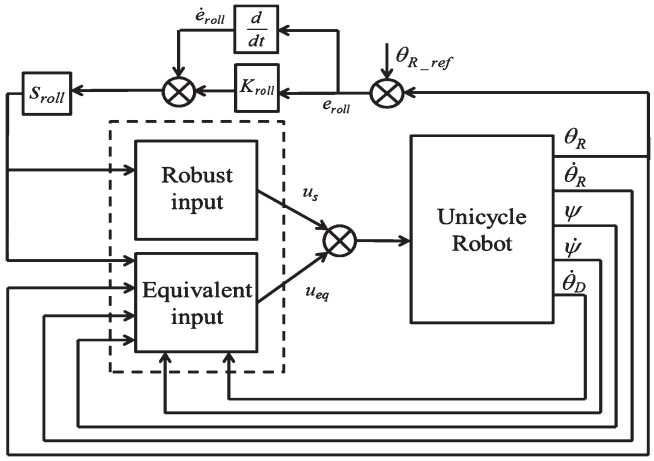

Fig. 5. Block diagram of the sliding-mode control of the roll controller.

the block diagram of a sliding-mode controller designed for the roll axis. The sliding surface of the roll control is defined as [17]–[19]

$$s_{\text{roll}} = K_{\text{roll}} e_{\text{roll}} + \dot{e}_{\text{roll}} \tag{30}$$

where $K_{\text{roll}} > 0$ is a design constant, and e_{roll} is the difference between the reference input and the current roll angle, which is defined as

$$e_{\text{roll}} = \theta_R - \theta_{R\_\text{ref}}. \tag{31}$$

The time derivative of s_{roll} is used to find the equivalent input, i.e., u_{eq}, as follows:

$$\begin{aligned} \dot{s}_{\text{roll}} &= K_{\text{roll}} \dot{e}_{\text{roll}} + \ddot{e}_{\text{roll}} \\ &= K_{\text{roll}} \dot{e}_{\text{roll}} + \ddot{\theta}_R - \ddot{\theta}_{R\_\text{ref}} \end{aligned} \tag{32}$$

where $\ddot{e}_{\text{roll}} = \ddot{\theta}_R - \ddot{\theta}_{R\_\text{ref}}$, and $\ddot{\theta}_R$ can be obtained from the dynamic equations expressed in terms of voltage inputs. The simplified dynamics of $\ddot{\theta}_R$ is obtained from (13) and (15) as follows:

$$\begin{aligned} \ddot{\theta}_R = \Big[& -J_d M_2(-L^2\theta_R - 2LR_w\theta_R)\dot{\theta}_R \\ & - J_d\left(M_2L^2\psi + M_3(-4L^2\psi - 2LR_w\psi)\right)\dot{\psi} \\ & - J_d\left(M_1 g R_w\theta_R + M_2 g(R_w\theta_R + L\theta_R)\right. \\ & \left. + M_3 g(R_w\theta_R + 2L\theta_R)\right) \\ & -2\alpha J_d V + 2J_d\beta(\dot{\theta}_D - \dot{\theta}_R)\Big] / D_{\text{roll}} \\ = \bar{f}(\theta_R, \dot{\theta}_R) & - \bar{g}_{\text{roll}} u_{\text{roll}} + F_u \end{aligned} \tag{33}$$

where $f(\theta_R, \dot{\theta}_R) = [-J_d M_2(-L^2\theta_R - 2LR_w\theta_R)\dot{\theta}_R - J_d(M_1 g R_w\theta_R + M_2 g(R_w\theta_R + L\theta_R) + M_3 g(R_w\theta_R + 2L\theta_R)) - 2J_d\beta\dot{\theta}_R]/D_{\text{roll}}$ $\bar{f}(\theta_R, \dot{\theta}_R)$ is a nominal value of $f(\theta_R, \dot{\theta}_R)$, $\bar{g}_{\text{roll}}$ denotes the nominal value of g_{roll}, $F_u = [-J_d(M_2L^2\psi + M_3(-4L^2\psi + F_d - 2LR_w\psi)\dot{\psi} + 2J_d\beta\dot{\theta}_D + \Delta f]/D_{\text{roll}}$, F_d is an external disturbance, and Δf is a modeling error. Letting $\dot{s} = 0$, the control input, which is called an equivalent input,

i.e., $u_{\rm eq}$, makes both $e_{\rm roll}$ and $\dot{e}_{\rm roll}$ to be null. $u_{\rm eq}$ is derived as follows:

$$u_{\rm eq} = -\frac{1}{\bar{g}_{\rm roll}}\left[K_{\rm roll}\dot{e}_{\rm roll} - \ddot{\theta}_{R\_\rm ref} + \bar{f}(\theta_R, \dot{\theta}_R)\right] \quad (34)$$

$$u_s = -\gamma_{\rm roll}\,\mathrm{sgn}(s_{\rm roll})/\bar{g}_{\rm roll} \quad (35)$$

where $\gamma_{\rm roll}$ is a strictly positive design constant, and sgn is the signum function. The Lyapunov function is defined as follows:

$$V = \frac{1}{2}s_{\rm roll}^2. \quad (36)$$

The time derivative of (36) using (32)–(35) can be given as follows:

$$\dot{V} = s_{\rm roll}\dot{s}_{\rm roll} = -\gamma_{\rm roll}|s_{\rm roll}| \le 0. \quad (37)$$

Therefore, $\dot{V}$ is negative for all $s_{\rm roll} \neq 0$. This means that $s_{\rm roll} \to 0$ as $t \to \infty$. The reaching condition is then satisfied [17], and the steady-state tracking performance can be guaranteed by (30) with a positive parameter $K_{\rm roll}$. Therefore, it is proved that $e_{\rm roll} \to 0$ as $t \to \infty$. However, the control law of (35) is discontinuous across $s_{\rm roll}(t)$. This leads to chattering in the control input and may excite high-frequency system dynamics. Thus, a sigmoid function, i.e., $\tanh(s_{\rm roll})$, is employed as the switching function to reduce the chattering phenomenon [25]. The roll control input is the sum of the equivalent input and a robust control input, which is the sum to make the system stable. Equation (35) is replaced by the following control:

$$u_s = -\gamma_{\rm roll}\tanh(s_{\rm roll}). \quad (38)$$

Therefore, for the roll attitude tracking of the unicycle robot, the desired control performance can be obtained without excessive chattering using the sliding-mode controller.

IV. Experiments

A. Descriptions of Experimental Equipment

The inertial-measurement-unit sensor is placed at the center of the body to simultaneously get the pitch and roll angles of the robot. At the center of the body, the coordinates of the roll and pitch axes are defined. The sensory data are transmitted to the main microcontroller unit (LM3S8962) through the RS-232 communication channel every 10 ms. For the roll and pitch control, Maxon dc motors are utilized to rotate the disk of the top and the wheels of the bottom. The dc motors are driven by an NT-DC20A H-bridge-type drive. The motor torque and the rotation speed are controlled by the PWM signal from the drive.

B. Switching Function

It is known that the sliding-mode controller with a signum switching function causes chattering in the control input. Therefore, to reduce chattering, a hyperbolic tangent function, which is a kind of sigmoid function, is used in this paper as a switching function in (38). The effect of chattering reduction by the sigmoid function is illustrated in Fig. 6. When the signum function is used as the switching function, the system finally becomes unstable because high-frequency robot dynamics is excited owing to chattering.

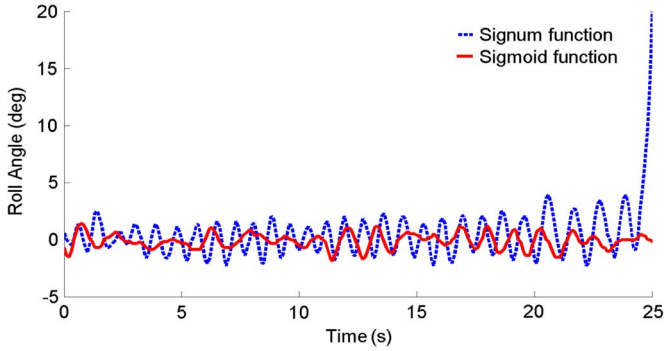

Fig. 6. Balancing control data with sigmoid and signum functions.

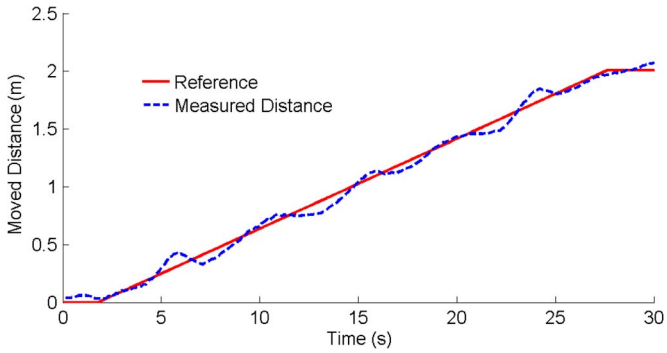

Fig. 7. Measured distance data with straight-line driving.

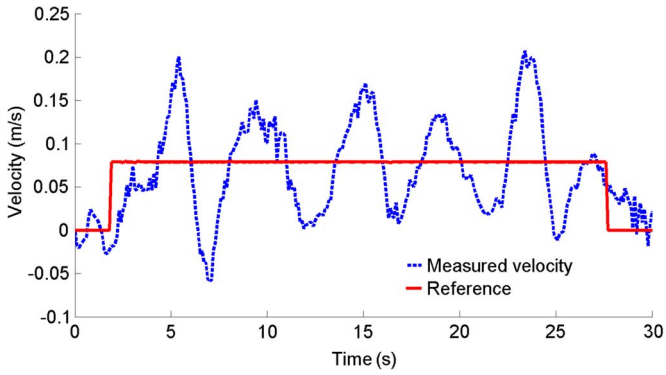

Fig. 8. Measured velocity data with straight-line driving.

The control performance of the single-wheel robot has been checked for a straight-line motion with a step velocity command and the desired velocity profile. For each experiment, the roll and pitch angles are measured and displayed to show the stability of the unicycle robot during driving.

C. Step Velocity

In Fig. 7, the solid line represents the distance of the mobile robot from the origin for the given step velocity input, and the broken line represents the real distance for 30 s of driving. Fig. 8 illustrates the desired and actual velocities of the unicycle robot with the proposed control algorithm for a step command input of 0.08 m/s. The velocity-tracking performance could not be very good because the unicycle robot should maintain its balance while trying to follow the desired velocity trajectory. However, comparing the result of Fig. 8 with that of the work in [26], it has been observed that the frequency of the

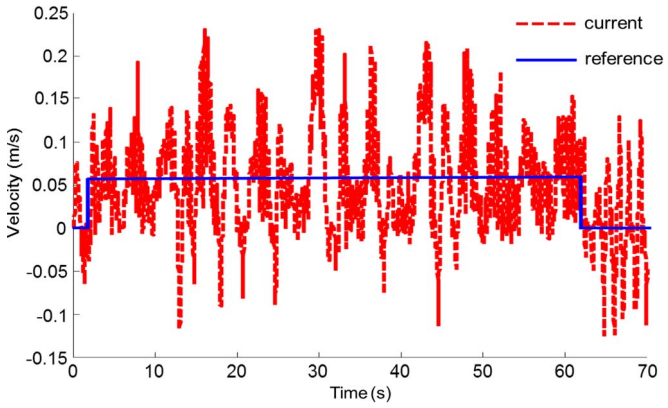

Fig. 9. Velocity data for the step input using the decoupled dynamic model.

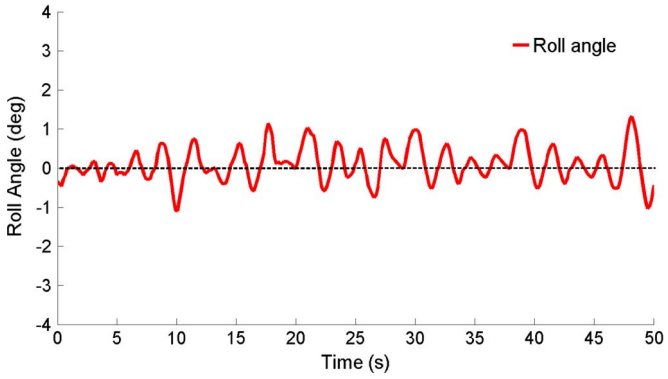

Fig. 10. Measured roll angle data with straight-line driving.

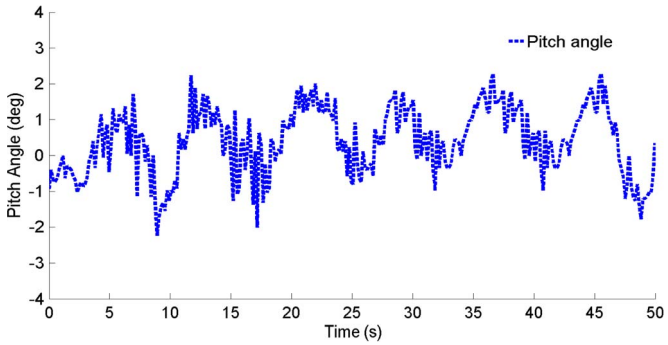

Fig. 11. Measured pitch angle data with straight-line driving.

velocity-tracking error is lower, and the magnitude is smaller with the proposed algorithm than with the previous algorithm using the decoupled dynamic model (see Fig. 9).

Fig. 10 represents the changes of the roll angle during the straight-line motion. The roll angle is kept within $\pm 2^\circ$, which is one of the main reasons for the velocity-tracking error. Fig. 11 illustrates the pitch angle error while the unicycle robot is driving to the goal. The errors are kept within $\pm 2.5^\circ$. The pitch control error is coupled to the roll control effort. That is, while the unicycle robot is maintaining its balance, it is not capable of controlling its driving speed precisely. Notice that the pitch angle has a small positive value for forward driving. A slightly forward-tilted posture is effective for the forward motion if the tilt angle can be controlled precisely.

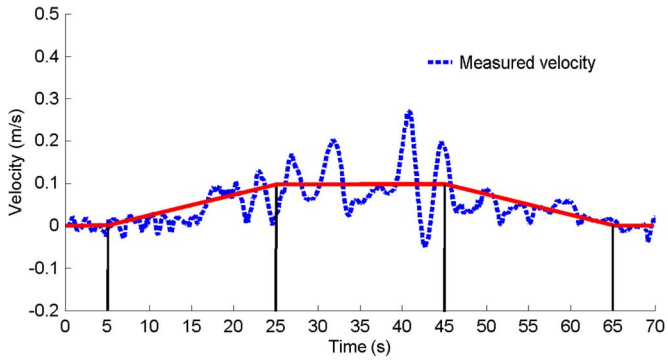

Fig. 12. Measured velocity data with speed-controlled driving.

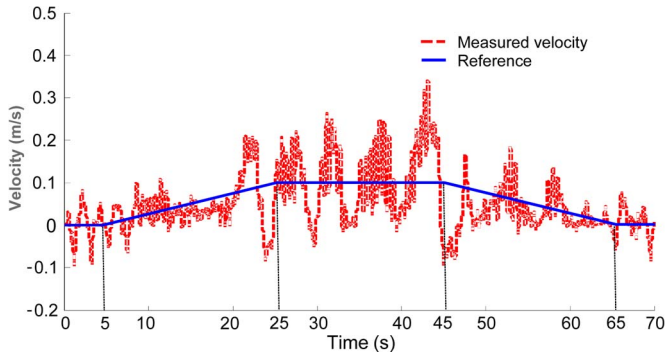

Fig. 13. Velocity data using the decoupled dynamic model.

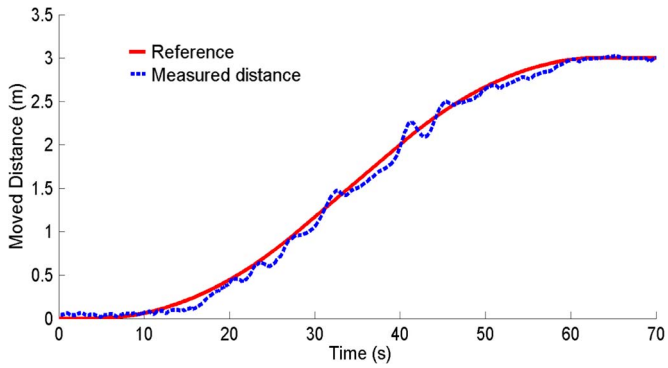

Fig. 14. Measured distance data with speed-controlled driving.

D. Trapezoidal Velocity Profile

To generalize the velocity control, it is planned to impose the trapezoidal velocity profile on the unicycle robot (see the solid line in Fig. 12). The first and last 5 s in Fig. 12 are used for stabilizing the unicycle robot. From 5 to 25 s, the velocity is increased linearly, whereas from 45 to 65 s, the velocity is decreased linearly. Between 25 and 45 s, the velocity is planned to be constant.

Fig. 12 illustrates the velocity-tracking performance of the proposed algorithm. The solid line is for the reference velocity, and the dashed line is for the actual velocity. Note that the velocity-tracking performance is greatly improved compared with Fig. 13, which is obtained by decoupling the controls of the roll and pitch axes [26]. The improvement in the velocity-tracking performance is very similar to that of the step velocity input. Fig. 14 illustrates the planned and actual distances of

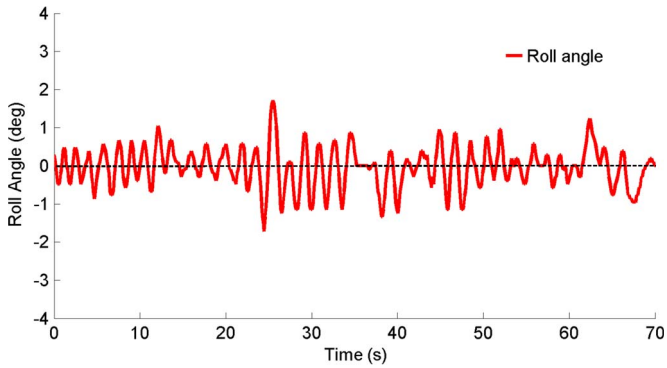

Fig. 15. Measured roll angle data with speed-controlled driving.

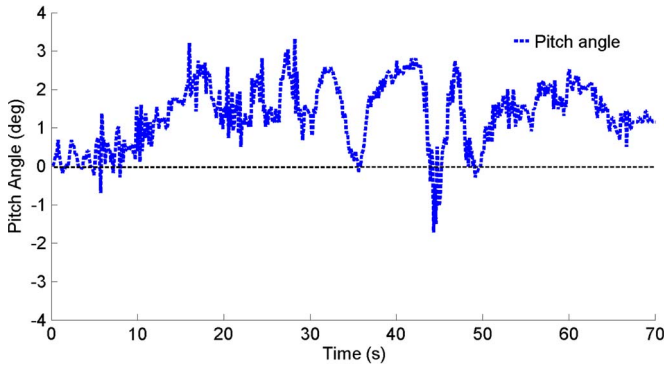

Fig. 16. Measured pitch angle data with speed-controlled driving.

the unicycle robot from the origin. The actual distance slightly deviated from the planned distance with time.

Fig. 15 illustrates that the roll axis error is stably maintained within $\pm 1.5^\circ$ while the unicycle robot is driving with the desired velocity profile. Although the velocity is increased, the roll angles are kept within a very stable range. Fig. 16 shows that the pitch angle is kept within $\pm 3^\circ$ with speed-controlled driving. The pitch vibration angle is bigger than the roll angle error since the pitch control is required for driving while maintaining a stable posture.

V. Conclusion

This paper has proposed a unified control system for the unicycle robot based on the derived dynamic model. For the control of left–right balance, roll axis control is implemented using the sliding-mode control algorithm, and velocity-tracking control is achieved by the pitch control using the LQR controller with a stable posture control. It is verified that the derived dynamic model includes complex coupling terms between the roll and pitch axes, which implies that the unified control system provides better velocity control performance than the previously proposed decoupled control algorithm. For the roll control, the sliding-mode controller is adopted, and the switching function employs the hyperbolic tangent function instead of the signum function to reduce chattering. With the step-input velocity and the trapezoidal velocity commands, the velocity-tracking performance of the proposed algorithm has been verified. With the unified and concurrent control of the roll and pitch axes, the velocity-tracking performance has greatly improved compared with that of the conventional decoupled control algorithm. Although the sigmoid function is utilized for the sliding-mode control of the roll axis, still, there was small chattering in the output. To minimize this chattering, a sliding-mode observer can be adopted as a future research work.

References

[1] I. Fantoni, R. Lozano, and M. Spong, "Energy based control of the Pendubot," *IEEE Trans. Autom. Control*, vol. 45, no. 4, pp. 725–729, Apr. 2000.
[2] J. Constantin, C. Nasr, and D. Hamad, "Control of robot manipulator and pendubot system using artificial neural networks," *Robotica*, vol. 23, no. 6, pp. 781–784, Nov. 2005.
[3] C. C. Tsai, C. K. Chan, S. C. Shih, and S. C. Lin, "Adaptive nonlinear control using RBFNN for an electric unicycle," in *Proc. IEEE Int. Conf. SMC*, 2008, pp. 2343–2348.
[4] A. Schoonwinkel, "Design and Test of a Computer Stabilized Unicycle," Ph.D. dissertation, Stanford Univ., Stanford, CA, USA, 1987.
[5] Z. Sheng and K. Yamafuji, "Postural stability of a human riding a unicycle and its emulation by a robot," *IEEE Trans. Robot. Autom.*, vol. 13, no. 5, pp. 709–720, Oct. 1997.
[6] J. O. Lee, S. I. Han, I. W. Han, S. I. Lee, and J. M. Lee, "Attitude and direction control of the unicycle robot using fuzzy-sliding mode control," *J. Inst. Control, Robot. Syst.*, vol. 18, no. 3, pp. 275–284, Mar. 2010.
[7] H. Jin, J. Hwang, and J. M. Lee, "A balancing control strategy for a one-wheel pendulum robot based on dynamic model decomposition: Simulations and experiments," *IEEE/ASME Trans. Mechatronics*, vol. 16, no. 4, pp. 763–768, Aug. 2011.
[8] S. H. Kim, J. O. Lee, J. Hwang, B. Ahn, and J. M. Lee, "Dynamic modeling and performance improvement of a unicycle robot," *J. Inst. Control, Robot. Syst.*, vol. 16, no. 11, pp. 1174–1181, Nov. 2010.
[9] H. Lim, J. Hwang, B. Ahn, and J. M. Lee, "Robust yaw motion control of unicycle robot," *J. Inst. Control, Robot. Syst.*, vol. 15, no. 11, pp. 1130–1136, Nov. 2009.
[10] CEATEC JAPAN 2008, [Online]. Available: http://www.ceatec.com/2008
[11] H. Ohsaki, M. Iwase, T. Sadahiro, and S. Hatakeyama, "A consideration of human-unicycle model for unicycle operation analysis based on moment balancing point," in *Proc. IEEE Int. Conf. Syst., Man, Cybern.*, Oct. 2009, pp. 2468–2473.
[12] S. C. Lin, C. C. Tsai, X. Q. Shih, and C. H. Lu, "Linearized two-loop posture and speed control of an electric unicycle," in *Proc. Int. Conf. Syst. Sci. Eng.*, 2010, pp. 245–250.
[13] A. Kadis, D. Caldecott, A. Edwards, and M. Jerbic, "Modelling, simulation and control of an electric unicycle," in *Proc. Australasian Conf. Robot. Autom.*, Dec. 2010, pp. 1–8.
[14] S. Zhiyu and L. Daliang, "Balancing control of a unicycle riding," in *Proc. 29th Chin. Control Conf.*, 2010, pp. 3250–3254.
[15] J. H. Lee, H. J. Shin, S. J. Lee, and S. Jung, "Novel air blowing control for balancing a unicycle robot," in *Proc. IEEE/RSJ Int. Conf. Intell. Robot. Syst.*, 2010, pp. 2569–2530.
[16] X. Ruan, X. Zhu, Y. Li, and R. Wei, "Lateral stabilization of a single wheel robot applying electromagnetic force," in *Proc. 10th World Congr. Intell. Control Autom.*, 2012, pp. 3675–3680.
[17] J. E. Slotine and W. Li, *Applied Nonlinear Control*. Englewood Cliffs, NJ, USA: Prentice-Hall, 1991.
[18] R. de Castro, R. E. Araujo, and D. Freitas, "Wheel slip control of EVs based on sliding mode technique with conditional integrators," *IEEE Trans. Ind. Electron.*, vol. 60, no. 8, pp. 3256–3271, Aug. 2013.
[19] C. Evangelista, P. Puleston, F. Valenciaga, and L. M. Fridman, "Lyapunov-designed super-twisting sliding mode control for wind energy conversion optimization," *IEEE Trans. Ind. Electron.*, vol. 60, no. 2, pp. 538–545, Feb. 2013.
[20] H. Li, J. Yu, C. Hilton, and H. Liu, "Adaptive sliding-mode control for nonlinear active suspension vehicle systems using T-S fuzzy approach," *IEEE Trans. Ind. Electron.*, vol. 60, no. 8, pp. 3328–3338, Aug. 2013.
[21] D. Ginoya, P. D. Shendge, and S. B. Phadke, "Sliding mode control for mismatched uncertain systems using an extended disturbance observer," *IEEE Trans. Ind. Electron.*, vol. 61, no. 4, pp. 1983–1992, Apr. 2014.
[22] D. Bernstein and W. Haddad, "Optimal output feedback for nonzero set points regulation," *IEEE Trans. Autom. Control*, vol. 32, no. 7, pp. 642–645, Jul. 1987.
[23] W. Haddad and D. Bernstein, "Optimal output feedback for non-zero set point regulation: The discrete-time case," *Int. J. Control*, vol. 47, no. 2, pp. 529–536, Feb. 1988.

[24] X. Ruan, Q. Wang, and N. Yu, "Dual-loop adaptive decoupling control for single wheeled robot based on neural PID controller," in *Proc. 11th Int. Conf. Control, Autom., Robot. Vis.*, Dec. 2010, pp. 2349–2354.
[25] J. B. Son, H. R. Kim, Y. S. Seo, and J. M. Lee, "PMSM sensorless speed control using a high speed siding mode observer," *J. Inst. Control, Robot. Syst.*, vol. 16, no. 3, Mar. 2010.
[26] J. O. Lee, S. I. Han, and J. M. Lee, "Decoupled dynamic control for pitch and roll axes of the unicycle robot," *IEEE Trans. Ind. Electron.*, vol. 60, no. 9, pp. 3814–3822, Sep. 2013.

Seong I. Han (M'12) received the B.S. and M.S. degrees in mechanical engineering and the Ph.D. degree in mechanical design engineering from Pusan National University, Busan, Korea, in 1987, 1989, and 1995, respectively.

From 1995 to 2009, he was an Associate Professor of electrical automation with Suncheon First College, Suncheon, Korea. He is currently with the Department of Electronics Engineering, College of Engineering, Pusan National University. His research interests include intelligent control, nonlinear control, robotic control, vehicle system control, and steel process control.

Jang M. Lee (SM'03) received the B.S. and M.S. degrees in electronic engineering from Seoul National University, Seoul, Korea, in 1980 and 1982, respectively, and the Ph.D. degree in computer engineering from the University of Southern California, Los Angeles, CA, USA, in 1990.

Since 1992, he has been a Professor with the Department of Electronics Engineering, College of Engineering, Pusan National University, Busan, Korea. He was the Leader of the "Brain Korea 21 Project" of Pusan National University. His research interests include intelligent robotics, advanced control algorithms, and specialized environment navigation/localization.

Dr. Lee is former President of the Korean Robotics Society.